Soft Computing for Assessing the Quality of Colour Prints*

Antanas Verikas[1,2], Marija Bacauskiene[2], and Carl-Magnus Nilsson[1]

[1] Intelligent Systems Laboratory, Halmstad University,
Box 823, S-30118 Halmstad, Sweden
[2] Department of Applied Electronics, Kaunas University of Technology,
Studentu 50, LT-51368, Kaunas, Lithuania
antanas.verikas@ide.hh.se/marija.bacauskiene@ktu.lt/cmn@ide.hh.se

Abstract. We present a soft computing techniques based option for assessing the quality of colour prints. The values of several print distortion attributes are evaluated by employing data clustering, support vector regression, and image analysis procedures and then aggregated into an overall print quality measure using fuzzy integration. The experimental investigations performed have shown that the print quality evaluations provided by the measure correlate well with the print quality rankings obtained from the experts. The developed tools are successfully used in a printing shop for routine print quality control.

1 Introduction

Offset lithographic printing is the most widely used commercial printing technology. Multicolour pictures in offset lithographic printing are represented by cyan (C), magenta (M), yellow (Y), and black (K) dots of varying sizes on thin metal plates. The two left-most images in Fig. 1 provide an example of an image taken from an offset-printed picture and an enlarged view of a small area of the picture, respectively. The four-colour dots are clearly seen in this figure. An image comprised of such dots is usually called a halftone image. Since four colours are used in the printing process, four halftone images are created.

Fig. 2 illustrates the flowchart of the graphical process resulting into a newspaper page. A colour camera and a scanner are the main tools used to obtain colour images that are later used in offset colour printing. The images, called original in this paper, are usually recorded in the RGB colour space, see Fig. 2. Since C, M, Y, and K colours are used to print colour pictures, the so-called colour separation process, converting images from the RGB to the CMYK colour space, is applied. Next, by applying some half-toning procedure, each of the obtained C, M, Y, and K images is converted into the halftone counterpart. Printing plates are then easily obtained from the halftone images by applying the so-called computer-to-plate (CTP) technology. The colour observed in a small local area of such pictures depends on the actual proportions of the amount of the four

* We gratefully acknowledge the support we have received from the Foundation for Knowledge and Competence Development, Sweden.

M. Ali and R. Dapoigny (Eds.): IEA/AIE 2006, LNAI 4031, pp. 701–710, 2006.

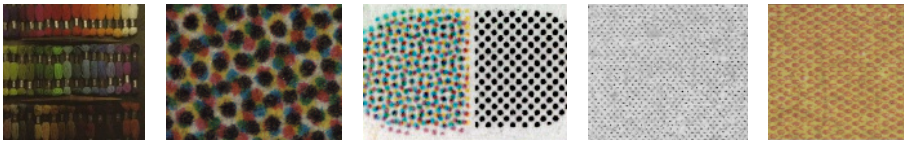

Fig. 1. A newspaper picture and an enlarged view of a small part of the picture (*left*). An example of the double grey-bar (*middle*). Two images exemplifying various quality aspects of printed dots (*right*).

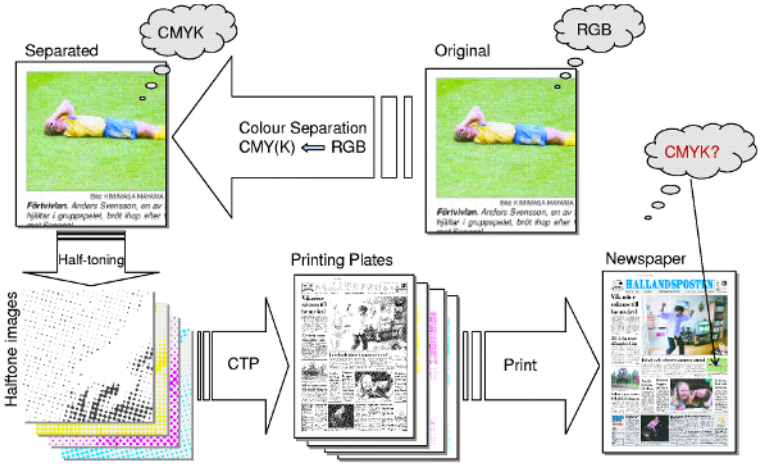

Fig. 2. The flowchart of the graphical process

inks deployed on that local area of paper—the CMYK values,—which have to be estimated by performing some measurements on the printed result (observe the question mark in Fig. 2). To obtain high quality prints, a relatively high precision of maintaining the beforehand determined ink proportions is required. The ability to print dots of the desired constant quality—size, shape, the degree of periodicity, ink density—is a key factor in obtaining the desired ink proportions in a small local area. The two rightmost images presented in Fig. 1 illustrate quality variations of printed dots. Thus, to assure high quality prints, a procedure for automatic print quality assessment is required. To enable the measurements required for assessing the print quality, a small test area is usually printed. Fig. 1 (*middle*) presents an example of such an area, the co-called double grey-bar.

Nonetheless of the current practice of using manual inspection of overall quality of complex colour prints in the printing industry, image analysis techniques are increasingly used for assessing various quality aspects of prints. Since manual procedures are tedious, time consuming, and the results are subjective as they depend on personal skills and mood, automated printing quality inspection systems are highly appreciated.

In general, various parameters are used to characterize print quality. The ones used most often are: ⋆ *dot deformation*—roundness, the degree of periodicity;

⋆ *dot gain*—the difference between the supposed average dot size and the actual measured average dot size; ⋆ *ink density deviation* from the required density level; ⋆ *edge sharpness*—the clarity of detail; ⋆ *the number of missing dots* (the parameter is only important in rotogravure printing).

A system attempting to simulate human print quality assessment for simple prints made by laser and ink jet printers is presented in [1]. Using simple print features characterizing noise level, edge sharpness, and tonal contrast the system is trained to categorize the prints into the "*bad quality*" and "*good quality*" classes. Another approach to the categorization of prints into the two classes was proposed in [2]. The categorization is based on moment invariants computed from a colour image histogram. A simple technique for measuring graininess when assessing print quality is presented in [3]. In [4], an approach to estimating the proportions of the four printing inks in a halftone image area was developed and used for printing quality monitoring in offset lithographic printing. Although there is a great interest in having a print quality measure integrating various quality aspects, the attempts to devise such a measure are very infrequent [5].

This paper is concerned with an attempt to develop such a measure for assessing the quality of offset lithographic prints. Several attributes characterizing distortion level of colour prints are estimated by employing data clustering, support vector regression, and image processing techniques and then aggregated into a print quality measure via Choquet fuzzy integral. To assess the offset printing quality we use the following print distortion attributes: the deviation of the *amount of C,M,Y,K inks* from the desired level, the *noise level*, the coefficient of variation of the *shape factor* of printed dots, the coefficient of variation of the *size* of the dots, and the coefficient of variation of *ink density*.

2 Estimating the Distortion Attributes

An image taken from a double grey-bar, as that shown in Fig. 1, is used as an information source to estimate the print distortion attributes. To evaluate the last three attributes, separate printed dots need to be detected and analyzed, while only a global analysis is required to estimate the first two. Next, we describe the main topics of the approach.

2.1 Estimating the Deviation of the Amount of Inks

The desired amount of the C, M, Y, and K inks in known in advance. Thus, estimation of the deviation amounts to estimation of the actual amounts of the inks. The average RGB values registered on the "black" part of the double grey-bar is the input information for estimating the amount of K. The amount of C, M, and Y is estimated from the average RGB values registered on the "coloured" part of the bar. Consequently, two mappings: $RGB \Rightarrow CMY$ and $RGB \Rightarrow K$ need to be determined. Since we use the approximately uniform $L^*a^*b^*$ colour space in the analysis, the mappings sought are $L^*a^*b^* \Rightarrow CMY$ and $L^*a^*b^* \Rightarrow K$. The $L^*a^*b^*$ values are easily obtained from RGB by applying the well known equations [6].

We use the support vector regression to discover the mappings sought. Let us assume that we have N colour patches spread over the whole colour gamut in question with known $L^*a^*b^*$—$\mathbf{x}$—and CMY—$\mathbf{y}$—values, the training set $S = \{(\mathbf{x}_1, \mathbf{y}_1), ..., (\mathbf{x}_N, \mathbf{y}_N)\}$. We collect the $\mathbf{x}$ vectors into the $N \times 3$ matrix $\mathbf{X}$ and the y vectors into the $N \times 3$ matrix $\mathbf{Y}$. Since we use the 1-norm ε-insensitive support vector regression, the optimization task is then to find $\boldsymbol{\alpha}^*$ by maximizing [7]

$$W(\boldsymbol{\alpha}) = \sum_{i=1}^{N} \alpha_i y_i - \varepsilon \sum_{i=1}^{N} |\alpha_i| - \frac{1}{2} \sum_{i,j=1}^{N} \alpha_i \alpha_j \kappa(\mathbf{x}_i, \mathbf{x}_j) \tag{1}$$

subject to

$$\sum_{i=1}^{N} \alpha_i = 0, \quad -C \leq \alpha_i \leq C, \quad i = 1, ..., N \tag{2}$$

with $\kappa(\mathbf{x}_i, \mathbf{x}_j)$ being a kernel, y_i is the target, and $C > 0$ is the regularization constant. Observe that a one-dimensional output is assumed in the above equations. The function f implementing the 1-norm ε-insensitive support vector regression is then given by

$$f(\mathbf{x}) = \sum_{j=1}^{N} \alpha_j^* \kappa(\mathbf{x}_j, \mathbf{x}) + b^* \tag{3}$$

where

$$b^* = -\varepsilon + y_i - \sum_{j=1}^{N} \alpha_j^* \kappa(\mathbf{x}_i, \mathbf{x}_j) \tag{4}$$

`for` i `such that` $0 < \alpha_i^* < C$.

In this study, we used polynomial $\kappa_p(\mathbf{x}_i, \mathbf{x}_j)$ and Gaussian $\kappa_g(\mathbf{x}_i, \mathbf{x}_j)$ kernels:

$$\kappa_p(\mathbf{x}_i, \mathbf{x}_j) = (1 + \mathbf{x}_i^T \mathbf{x}_j)^d \tag{5}$$

$$\kappa_g(\mathbf{x}_i, \mathbf{x}_j) = \exp\{-||\mathbf{x}_i - \mathbf{x}_j||^2/\sigma\} \tag{6}$$

with d and σ being parameters of the kernels. The mapping $L^*a^*b^* \Rightarrow K$ is found likewise, except that the output is one-dimensional.

The C, M, Y, and K values range between 0 and 100, where 0 means no ink and 100 stands for the area entirely covered by ink. Having the C, M, Y, and K values estimated, the distortion attribute Q_1 is then given by the average difference between the desired and the estimated actual values of the amount of inks.

2.2 Estimating the Noise Level

The "black" part of the bar is utilized to estimate the noise level. The estimation is based on the analysis of the Fourier power spectrum $P(u, v) = \| F(u, v) \|^2 = R^2(u, v) + I^2(u, v)$ of a "dot image" $f(x, y)$, with $F(u, v)$ being the Fourier

transform of $f(x, y)$, and $R(u, v)$ and $I(u, v)$ are the real and imaginary components of $F(u, v)$, respectively. First, the central part of the power spectrum is eliminated and three highest power peaks are then found in the upper part—the first and the second quadrants—of the power plain.

Next, the power spectrum in the neighbourhood of each detected peak is normalized to build a probability density function $p(\xi)$. Finally, the averaged entropy, given by Eq.(7), is computed and used as a distortion attribute Q_2 to quantify the noise level.

$$Q_2 = H = -\frac{1}{3 \log N_N} \sum_{j=1}^{3} \sum_{i=1}^{N_N} p_j(\xi_i) \log[p_j(\xi_i)] \tag{7}$$

where N_N is the size of the neighbourhood. Higher entropy H values are usually computed for images of less regular dots.

2.3 Detecting the Printed Dots

We solve the task through unsupervised colour image segmentation. A relatively simple fuzzy-clustering-based image segmentation technique can be used to segment an image taken from the "black" part of the bar [8]. However, a more involved analysis is required to accurately segment the coloured part of the bar. Eight combinations: *cyan*, *magenta*, *yellow*, *white*, *green* (*cy*), *blue* (*cm*), *red* (*my*), and *black* (*cmy*) are possible when printing C, M, and Y dots on each other. Thus, the coloured part is segmented into these eight colour classes. Having the segmentation results, the C, M, and Y dots are easily recovered.

We segment an image by applying the mean shift procedure [9]. Pixels of a colour image create a density distribution in the $L^*a^*b^*$ space. Pixels of similar colours create modes of the distribution. If we can associate with each pixel of the image the closest local mode of the distribution, we can use this information to segment the image. The mean shift procedure provides this association.

Let us assume that $\{\mathbf{x}_i\}, i = 1, ..., N$ is a set of image pixels and $S_h(\mathbf{x})$ denotes a hyper-sphere of radius h centered on $\mathbf{x}$ and containing $N_\mathbf{x}$ pixels. Then $M_h(\mathbf{x})$ given by

$$M_h(\mathbf{x}) = \frac{1}{N_\mathbf{x}} \sum_{\mathbf{x}_i \in S_h(\mathbf{x})} \mathbf{x}_i - \mathbf{x} \tag{8}$$

is called the *sample mean shift* [9]. The mean shift vector points towards the maximum increase of the density. Thus, the mean shift procedure, obtained by successive computation of $M_h(\mathbf{x})$ and translation of the window $S_h(\mathbf{x})$ by $M_h(\mathbf{x})$ produces a path leading to a local density mode—convergence point. Each pixel is associated with a convergence point representing a local density mode in the 3-dimensional space. The convergence points of the procedure serve as seed points for performing image segmentation. To obtain homogenous regions in the segmented image, sufficiently close convergence points are merged. We do the segmentation in the concatenated 5–dimensional *spatial-range* space. There are two dimensions—x, y—in the spatial and three—$L^*a^*b^*$—in the range space.

Having the printed dots detected, the distortion attribute Q_3, related to dot size, is given by the coefficient of variation of the size

$$Q_3 = \sigma_S / m_S \tag{9}$$

with σ_S and m_S being the standard deviation and the mean value of the dot size S, respectively.

2.4 Estimating the Ink Density

We measure ink density with a colour camera via the local kernel ridge regression based reconstruction of a reflectance spectrum of a sample being measured [10]. Having the spectrum, the ink density D is evaluated as

$$D = -\lg \frac{\sum R(\lambda) S(\lambda) F(\lambda)}{\sum S(\lambda) F(\lambda)} \tag{10}$$

where λ stands for a wavelength, $R(\lambda)$ is the reflectance spectrum of a sample, $S(\lambda)$ is the relative power distribution of the light source, and $F(\lambda)$ is the spectral transmittance of the densitometer filter. The ink density is estimated for each printed dot and the distortion attribute Q_4, related to ink density, is then given by the coefficient of variation of the density $Q_4 = \sigma_D / m_D$.

2.5 Shape Factor

The dot shape factor ϑ we use is given by

$$\vartheta = S_d / P_d \tag{11}$$

where S_d and P_d are the dot area and perimeter, respectively. The distortion attribute Q_5, related to dot shape, is given by the coefficient of variation of the shape factor $Q_5 = \sigma_\vartheta / m_\vartheta$.

3 Fuzzy Integration of Distortion Attributes

In practice, distortion attributes are usually highly correlated. Therefore, when aggregating them into a quality measure it is desirable to assign weights not only to individual attributes, but also to groups of them. Aggregation based on fuzzy integrals—fuzzy integration—possesses this valuable property. In such schemes, different attributes are fused into a final quality measure by a fuzzy integral with respect to a fuzzy measure. A fuzzy measure represents weights on each attribute and also weights on each group of attributes.

3.1 Fuzzy Measure and Fuzzy Integral

Let Z be a non-empty finite set—a set of distortion attributes in our case—and 2^Z the power set of Z. A set function $g : 2^Z \to [0, 1]$ is a *fuzzy measure* if • $g(\emptyset) = 0$; $g(Z) = 1$ and • if $A, B \subset 2^Z$ and $A \subset B$ then $g(A) \leq g(B)$.

The λ-fuzzy measure. Sugeno [11] introduced the so called λ-fuzzy measure, which satisfies the following additional property

$$g(A \cup B) = g(A) + g(B) + \lambda g(A)g(B) \tag{12}$$

for all $A, B \subset Z$ and $A \cap B = \emptyset$, and for some $\lambda > -1$. Let $Z = \{z_1, z_2, \ldots, z_L\}$ be a finite set, where L is the number of distortion attributes, and let $g^i = g(\{z_i\})$. When g is the λ-fuzzy measure, the values of $g(A_i)$ can be computed recursively:

$g(A_1) = g(\{z_1\}) = g^1$, $g(A_i) = g^i + g(A_{i-1}) + \lambda g^i g(A_{i-1})$, for $1 < i \leq L$.

We use the *discrete Choquet integral* to make the fuzzy integration. The discrete Choquet integral of a function h with respect to g is defined as

$$C_g(h(z_1), \ldots, h(z_L)) = \sum_{i=1}^{L} [h(z_i) - h(z_{i-1})] g(A_i) \tag{13}$$

where indices i have been permuted so that $0 \leq h(z_1) ... h(z_L) \leq 1$, $A_i = \{z_i, ..., z_L\}$; $h(z_0) = 0$. In our case, the function $h(z)$ is a function of values of the distortion attributes. We adopted the following function $h(Q_i)$:

$$h(Q_i) = \exp\{-\theta_i Q_i\} \tag{14}$$

where θ_i is a parameter.

The g^i value reflects the importance of the ith distortion attribute. In this paper, the value was chosen to be proportional to the Spearman's correlation coefficient ρ between the quality rankings provided by the attribute and the expert. To evaluate the ranking obtained from the overall quality measure, we also used the Spearman's correlation coefficient:

$$\rho = \frac{\sum_{t=1}^{T} R[M(t)]R[E(t)] - T\left(\frac{T+1}{2}\right)^2}{\sqrt{\sum_{t=1}^{T} R^2[M(t)] - T\left(\frac{T+1}{2}\right)^2} \sqrt{\sum_{t=1}^{T} R^2[E(t)] - T\left(\frac{T+1}{2}\right)^2}} \tag{15}$$

where T is the number of images used, $R[E(t)]$ and $R[M(t)]$ are the quality rank given to the tth image by the expert and the measure, respectively.

4 Experimental Investigations

The experimental tests performed concern an offset newspaper printing process. An on-line printing process monitoring system has been used to capture the images of test areas used in the experiments. The system is equipped with a CCD colour camera of 1600×1200 pixels. The camera can be positioned with a high accuracy at any point across a newspaper page and is able to record high quality well-focused colour images from a web running at up to 15 m/s speed. An off-line version of the system is also available.

4.1 Choice of Parameters

The width of the kernel $\sigma = 0.2$ and the polynomial degree $d = 2$ turned to be a good choice for the kernel parameters. The value of the regression insensitivity parameter ε was chosen based on the process knowledge and was set to $\varepsilon = 0.015$. The regularization constant C was found by cross-validation and was equal to $C = 50$. Based on the values of the correlation coefficient ρ, the following importance weights g^i have been given to the the distortion attributes: $g^1 = 0.5$, $g^2 = 0.8$, $g^3 = 0.2$, $g^4 = 0.4$, and $g^5 = 0.2$. The values of $\theta_1 = 2$, $\theta_2 = 5$, $\theta_3 = 2$, $\theta_4 = 4$, and $\theta_5 = 2$ worked well in all the tests performed.

4.2 Estimating the Amount of Ink

To learn the mappings $L^*a^*b^* \Rightarrow CMY$ and $L^*a^*b^* \Rightarrow K$, a set of test colour patches were printed keeping the same ink density. For each cyan, magenta, and yellow inks, the average nominal ink coverage of a patch area—the dot size—was varied in 20% steps, namely, 0, 20, 40, 60, 80, and 100%. An example of 216 such pathes, with C, M, and Y varying from 0 to 100%, is shown in Fig. 3. The average ink coverage for the black ink was varied in 3% steps from 0 to 100%. In total, 216 test colour and 34 black patches were designed. Data from five of such prints were automatically recorded using the on-line system. One set of the data has been used to estimate the regression parameters, while the other four sets were allocated for testing.

Fig. 3. An image taken from the 216 colour patches

Colour	Gaussian	Polynom
C	1.12 (0.60)	1.17 (0.22)
M	1.09 (0.56)	1.18 (0.61)
Y	1.36 (0.77)	1.47 (0.59)
K	0.55 (0.37)	0.64 (0.39)

Fig. 4. The average prediction error of the C, M, Y, and K values

To learn the mappings, the target values—the actual C, M, Y, and K values—are to be known. Though the nominal C, M, Y, and K values used to print the test patches are known, the actual values remain unknown, since halftone dots grow during the printing process. We estimated these values from the RGB values of the halftone series of the pure colours.

Fig. 4 presents the average absolute prediction error of the actual C, M, Y, and K values for the test data set using the Gaussian and polynomial kernels. In the parentheses, the standard deviation of the error is provided. Observe that C, M, Y, and K values range from 0 to 100. The prediction accuracy obtained is high

enough for the approach to be used in practical applications. It is worth noting that evaluation of the prediction error is not an easy task, since the ground truth is not known. The actual C, M, Y, and K values used to estimate the regression parameters were evaluated using patches of single colours only (no overprints). Let us assume that the actual value of C=28 has been evaluated for the nominal C=20. It was then assumed that for all the overprints printed using the nominal value of C=20, the actual value of C was always 28, irrespective the proportions of the other two inks. It is clear that the assumption does not always holds in practice. Thus, we can expect that the estimation errors are even smaller, as the experience shows, than those observed in Fig. 4.

4.3 Assessing the Quality of Prints

The aim of the test was to compare the quality ranking given to different printed issues by human experts and by the integral quality measure. The quality of eight issues printed using different printing conditions and paper types has been ranked by 14 experts and the average ranking was obtained. Each issue contained test areas with the halftone bars. Images of the areas were recorded by the system and used to calculate the distortion attributes. The Spearman's correlation coefficient between the average ranking obtained from the expert and the rankings provided by the distortion attributes and the integral quality measure was then calculated.

Table 1 presents values of the correlation coefficient ρ computed for three distortion attributes yielding the highest values of the coefficient as well as the integral measure aggregating information available from all the attributes. The coefficient was evaluated separately for C, M, Y, and K inks. The Table also provides values of the probability p to obtain such correlation by chance.

Table 1. The Spearman's correlation coefficient ρ and the probability p.

Colour	Amount of Ink		Noise		Density		Integral	
	ρ	p	ρ	p	ρ	p	ρ	p
C	0.905	0.0020	0.976	0.0000	0.738	0.0366	0.976	0.0000
M	0.952	0.0003	0.976	0.0000	0.976	0.0000	0.952	0.0003
Y	0.929	0.0009	0.976	0.0000	0.738	0.0366	0.952	0.0003
K	0.905	0.0020	0.619	0.1017	0.905	0.0020	0.976	0.0000

The values of the Spearman's correlation coefficient computed for the rankings substantiate good correlation between the quality rankings obtained from the human experts and the overall quality measure. Lower values—not presented in Table 1—of the correlation coefficient were computed using rankings provided by the dot size and shape related attributes. A relatively low number of pixels, the printed dots consisted of, caused a rather high variance of the two aforementioned parameters. However, if the resolution is increased, the high variation of the dot size and shape seem to be good indicators of deficiencies in the printing process.

5 Conclusions

We presented a soft computing based option for assessing the quality of colour prints. Several attributes characterizing global as well as local distortion level of printed dots are estimated employing data clustering, support vector regression, and image processing techniques and then aggregated into an overall print quality measure via Choquet fuzzy integral.

The noise level, deviation of the actual amount of ink deposited on the paper from the desired level, and the variation coefficient of the average ink density level of different printed dots are the three most informative distortion attributes. Due to the relatively low resolution used to represent printed dots, the dot size and the shape related distortion attributes were less informative. However, if the resolution is increased, the high variation of the dot size and the shape become useful indicators of deficiencies in the printing process. The experimental investigations performed have shown that print quality evaluations provided by the proposed integral print quality measure correlate well with the print quality rankings obtained from the experts. The developed tools are successfully used in a printing shop for a routine print quality control.

References

1. Tchan, J., Thompson, R.C., Manning, A.: A computational model of print-quality perception. Expert Systems with Applications **17** (1999) 243–256
2. Luo, J., Zhang, Z.: Automatic colour printing inspection by image processing. Journal of Materials Processing Technology **139** (2003) 373–378
3. Trepanier, R.J., Jordan, B.D., Nguyen, N.G.: Specific perimeter: a statistic for assessing formation and print quality by image analysis. TAPPI Journal **81** (1998) 191–196
4. Verikas, A., Malmqvist, K., Bergman, L.: Neural networks based colour measuring for process monitoring and control in multicoloured newspaper printing. Neural Computing & Applications **9** (2000) 227–242
5. Verikas, A., Bacauskiene, M.: Image analysis and fuzzy integration applied to print quality assessment. Cybernetics and Systems **36** (2005) 549–564
6. Wyszecki, G., Stiles, W.S.: Color Science. Concepts and Methods, Quantitative Data and Formulae. 2nd edn. John Wiley & Sons, New York (1982)
7. Shawe-Taylor, J., Cristianini, N.: Kernel Methods for Pattern Analysis. Cambridge University Press, Cambridge, UK (2004)
8. Bergman, L., Verikas, A., Bacauskiene, M.: Unsupervised colour image segmentation applied to printing quality assessment. Image and Vision Computing **23** (2005) 417–425
9. Comaniciu, D., Meer, P.: Mean shift: A robust approach toward feature space analysis. IEEE Trans Pattern Analysis Machine Intelligence **24** (2002) 603–619
10. Verikas, A., Bacauskiene, M.: Estimating ink density from colour camera RGB values by the local kernel ridge regression. Engineering Applications of Artificial Intelligence **19** (2006)
11. Sugeno, M.: Fuzzy measures and fuzzy integrals: A survey. In Gupta, M.M., Saridis, G.N., Gaines, B.R., eds.: Fuzzy Automata and Decision Process. North-Holland Pub, Amsterdam (1977) 89–102